Comput Geosci (2016) 20:637–653
DOI 10.1007/s10596-015-9540-5

ORIGINAL PAPER

Integration of Markov mesh models and data assimilation techniques in complex reservoirs

M. Panzeri[1] · E. L. Della Rossa[2] · L. Dovera[2] · M. Riva[1,3] · A. Guadagnini[1,3]

Received: 12 January 2015 / Accepted: 8 October 2015 / Published online: 5 November 2015

Abstract We present a methodology that allows conditioning the spatial distribution of geological and petrophysical properties of reservoir model realizations on available production data. The approach is fully consistent with modern concepts depicting natural reservoirs as composite media where the distribution of both lithological units (or facies) and associated attributes are modeled as stochastic processes of space. We represent the uncertain spatial distribution of the facies through a Markov mesh (MM) model, which allows describing complex and detailed facies geometries in a rigorous Bayesian framework. The latter is then embedded within a history matching workflow based on an iterative form of the ensemble Kalman filter (EnKF). We test the proposed methodology by way of a synthetic study characterized by the presence of two distinct facies. We analyze the accuracy and computational efficiency of our algorithm and its ability with respect to the standard EnKF to properly estimate model parameters and assess future reservoir production. We show the feasibility of integrating MM in a data assimilation scheme. Our methodology is conducive to a set of updated model realizations characterized by a realistic spatial distribution of facies and their log permeabilities. Model realizations updated through our proposed algorithm correctly capture the production dynamics.

Keywords Markov mesh model · Data assimilation · Ensemble Kalman filter · History matching · Facies characterization

✉ M. Panzeri
marco.panzeri@polimi.it

[1] Department of Civil and Environmental Engineering, Politecnico di Milano, Piazza L. Da Vinci 32, 20133 Milan, Italy

[2] Eni - S.p.A. Via Emilia 1, 20097 San Donato Milanese, Milan, Italy

[3] Department of Hydrology and Water Resources, University of Arizona, Tucson, AZ 85721, USA

1 Introduction

Conditioning the spatial distribution of petrophysical properties of hydrocarbon reservoirs on field-scale production data is key step to (a) reducing the uncertainty associated with the assessment of the future performance of the reservoir and (b) developing effective strategies for enhanced hydrocarbon recovery. Increasing attention has been devoted to the development of ensemble data assimilation techniques due to their ability for real-time assimilation of field measurements. These are then employed to condition the generation of a collection of up-to-date reservoir model realizations that can be readily employed for production forecasting and decision making. In this sense, such techniques are typically based on a Monte Carlo scheme, where a finite number (usually referred to as an ensemble) of equally likely realizations is employed to quantify the uncertainty associated with the spatial distribution of model parameters and state variables in the target system. Among the available data assimilation methods, the ensemble Kalman filter (EnKF) [6, 12] has been shown to constitute an effective tool to characterize the spatial distribution of porosity and permeability of hydrocarbon reservoirs at a generally affordable computational cost (see [1] for a recent review). It is well known that EnKF is optimal when the

unknown model parameters and state variables form a multivariate Gaussian random field. However, most reservoir analyses require to explicitly take into account the complex internal architecture of the medium. The latter is composed by multiple lithological units (i.e., facies), which can be considered as distinctive and nonoverlapping regions of the host rock system with given characteristics such as porosity, permeability, and mineral composition. A common procedure to distinguish between diverse facies in a reservoir model relies on the use of indicator functions, which by their nature cannot be represented by Gaussian distributions.

Several techniques are nowadays available to generate multiple random realizations of facies spatial fields conditional on prior information on the internal geological architecture of the target reservoir. These include object-based (e.g., [8, 10, 25]) and process-based methods (e.g., [5, 14]), multiple-point geostatistics (MPS) techniques (e.g., [3, 32, 35]), and Markov mesh (MM) models (e.g., [7, 21, 31]). The use of EnKF to condition on production data the spatial distribution of facies in complex reservoirs is often fraught with difficulties [1, 27] and typically leads to a set of updated realizations that (a) are not consistent with available elements of prior knowledge about the internal system architecture and (b) do not provide a reliable basis for a proper prediction of future reservoir production and for an accurate uncertainty assessment.

Various approaches have been proposed to tackle this challenge. A common way of dealing with the problem relies on the application of a suitable transformation to the facies indicator functions and describes these in terms of normally distributed random fields. Integration of these techniques within the EnKF framework generally implies that (a) the EnKF model has to be formulated to update the transformed Gaussian variable and (b) the updated facies spatial fields are calculated through back/transformation to the original discrete space. Suitable transformation techniques coupled with EnKF for assimilating dynamic and hard data through a reservoir history matching procedure include, e.g., the truncated pluri-Gaussian method [22] employed by [4, 23, 24, 30], or the level set method which has been combined with EnKF by [26] under the assumption that the velocity governing the evolution of the level set function is a Gaussian random field. The discrete cosine transform (DCT) was also introduced in this context by [16]. These authors used EnKF to update the coefficients of the cosine basis functions which was employed to represent the spatial distribution of state variables and model parameters. [15] coupled EnKF with the uniform score transform and with the inverse standard Gaussian transform to (a) update a collection of random realizations generated from a uniform distribution and (b) use these as input for the generation based on multipoint methods of a set of updated facies fields.

A different strategy relies on a two-step approach according to which EnKF is first employed to update a continuous spatial field of target quantities, which is then followed by a post-processing step through which the updated variables are projected onto their original space composed by discrete geological units. This technique was first proposed by [28], who employed a Markov chain model to describe the uncertain spatial arrangement of facies within a one-dimensional domain and based the post-processing step on the Viterbi algorithm [34]. This technique was modified by [36] to extend its range of applicability to two-dimensional domains.

As an alternative to this technique, one can employ an approach structured on the following three steps: (a) averaging the permeability realizations over all members of the ensemble, (b) directly updating the resulting averaged field through EnKF without applying any transformation scheme, and (c) drawing a new set of updated facies realizations which are driven through the updated averaged field obtained at step (b). This procedure allows somehow conditioning the updated facies realizations on the updated averaged maps as well as on production data. In the context of reservoir history matching, this methodology was pioneered by [17]. These authors employed the EnKF scheme to update the sample average of the log permeability field and converted the latter into a facies probability map through a linear mapping function. The information associated with this updated probability map was then combined with the *snesim* algorithm [32] through the τ-model [18] to generate the updated collection of facies realizations.

Here, we present a new data assimilation algorithm that is conducive to conditioning on a set of measured production data the spatial distribution of facies and associated petrophysical properties of a collection of hydrocarbon reservoirs. The method we propose falls in the last category of approaches reviewed above. Unlike [17], here we employ a MM model to describe the spatial distribution of lithofacies within the domain of interest. This model is a subclass of Markov random fields that are defined on a regular path which scans all elements of the grid discretizing the domain of interest. Although the concept is not new (see, e.g., [2]), the use of a MM model for geological facies modeling has been introduced only in recent years [21, 31]. Interesting features of MM models as opposed to other algorithmically guided approaches are their consistent theoretical basis as well as the flexibility of honoring complex features. A detailed comparison between the MM and *snesim* approaches has been presented by [21, 31]. These authors have demonstrated that the MM approach compares favorably against the *snesim* approach in terms of quality of the generated facies fields and computational efficiency. The MM approach is intrinsically not suitable for generating realizations which are conditional on hard or dynamic data.

To the best of our knowledge, [19] present the only study on this aspect. In their work, MM is coupled with an indicator kriging approach to generate a collection of facies field realizations conditioned on a set of observed facies data. The development of a data assimilation algorithm capable of conditioning a MM model on a set of dynamic data is currently an open challenge.

The key element of novelty of our work consists on embedding the concept of MM models into an EnKF-based Monte Carlo history matching procedure. We test the proposed methodology by way of a synthetic reservoir model representing a complex geological system. We analyze the accuracy and computational efficiency of our algorithm and demonstrate its benefit with respect to the standard EnKF in predicting the forecast production. The work is organized as follows. Section 2 outlines the probabilistic model employed to describe the uncertain spatial distribution of the geological facies and of the associated petrophysical properties (i.e., the log permeabilities) within the domain of interest. Section 3 illustrates the proposed data assimilation scheme. Section 4 summarizes the results of the synthetic test case. Section 5 presents our conclusions.

2 Markov mesh model

The (randomly heterogeneous) spatial distribution of the geological facies in the system is handled by means of a Markov mesh (MM) model coupled with a multi-grid approach. The latter is adopted because of its ability to accurately delineate detailed facies geometries and complex spatial patterns distributed across multiple scales in a rigorous probabilistic framework. The formulation of our MM model is grounded on the concepts illustrated by [21, 31], to which we refer for the theoretical foundations of the approach. In this section, we illustrate the details concerning our implementation and the key theoretical aspects underpinning the way the MM model is embedded within a history matching workflow.

We define a unilateral path scanning all elements N_e of the grid onto which the model of the reservoir is discretized. A label $i \in \{1, \ldots, N_e\}$ is assigned to each grid cell during this scanning step. The conditional probability, $\pi\left(s_i \left| \mathbf{s}_{j<i} \right.\right)$, of observing a facies value, s_i, over a generic element i of the grid depends on the facies values associated with elements having index $j < i$, $\mathbf{s}_{j<i}$ [31], i.e.,

$$\pi\left(s_i \left| \mathbf{s}_{j<i} \right.\right) = \pi\left(s_i \left| \mathbf{s}_{\Gamma_i} \right.\right) = \frac{\prod_{k_f=1}^{K} \exp\left\{ s_i^{k_f} \mathbf{z}_i^{+} \theta_{l(i)}^{k_f} \right\}}{\sum_{k_f=1}^{K} \exp\left\{ \mathbf{z}_i^{+} \theta_{l(i)}^{k_f} \right\}} \tag{1}$$

Here, $s_i^{k_f}$ is the indicator variable of facies k_f over element i (i.e., $s_i^{k_f} = 1$ if $s_i = k_f$ and 0 otherwise); K is the total number of facies in the target system; Γ_i is a subset of the domain cells formed by cells with $i < j$; and the vector $\mathbf{s}_{\Gamma_i}$ contains the facies identifiers associated with the elements of Γ_i. The superscript "+" in Eq. 1 stands for transpose; $\mathbf{z}_i$ is a column vector of N_P+1 coefficients which depend on the facies distribution over Γ_i, where $N_P + 1$ is the number of parameters of the MM model. We define the elements of vector $\mathbf{z}_i$ following [31] and set each of the first N_P coefficients to 0 or 1 depending on whether a predefined pattern of facies is reproduced over Γ_i or not, while the last entry of $\mathbf{z}_i$ is always equal to unity. This formulation allows generating unconditional realizations of the random facies field by following the defined sequential path and by extracting a facies value at each grid element according to the conditional probabilities evaluated through (1). In our implementation, the MM model is then coupled with a multi-grid approach [21] according to which the domain is partitioned into L disjoint sets. The latter are conveniently defined in such a way that the grid elements belonging to each set allow detecting the features of the facies field associated with a given scale of interest. With this implementation, the geological patterns are initially reproduced at a coarse scale and are subsequently transferred to increasingly refined grids. Quantities $\theta_{l(i)}^{k_f}$ in Eq. 1 are vectors of unknown parameters that are defined for each facies value, $k_f = 1, \ldots, K$, and for each scale, $l(i) = 1, \ldots, L$, $l(i)$ being a function that allows identifying the scale which the element with label i belongs to. The values of these parameters play a critical role within the MM model and have a direct influence on the probability of occurrence of any possible spatial pattern associated with the random facies field. We follow [31] and take advantage of the observation that the conditional probability of detecting a facies field, $\mathbf{s}$, given the parameter vectors is expressed as the product of conditional probabilities evaluated at all grid elements, i.e.,

$$\pi\left(\mathbf{s} \left| \theta_1^1, \cdots, \theta_L^K \right.\right) = \prod_{i=1}^{N_e} \pi\left(s_i \left| \mathbf{s}_{\Gamma_i} \right.\right) \tag{2}$$

We then estimate the parameters of the MM model via maximum likelihood by means of a suitable training image. The latter should contain all relevant features one desires to preserve in the collection of realizations. Issues associated with the selection of training images as well as the influence of these on the final model result are widely discussed in the literature (e.g., [21]). Figure 1 provides a graphical depiction of the implemented scanning path and grid refinement and a snapshot of a simulation at the time element i is visited during the progression of the generation algorithm.

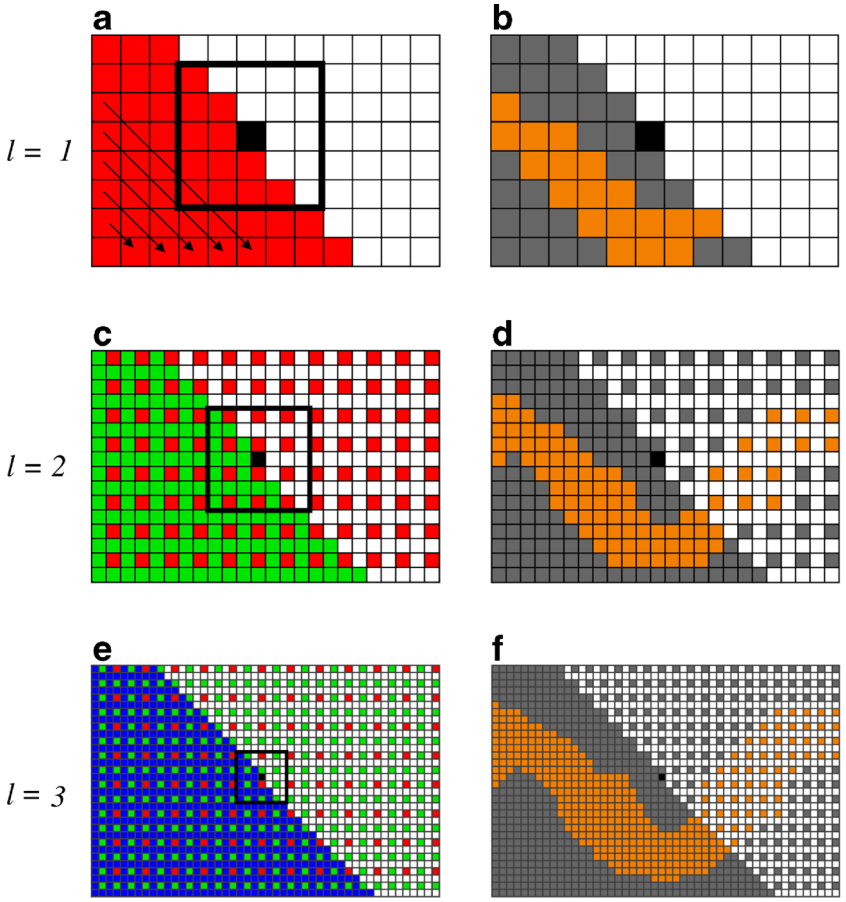

Fig. 1 Three snapshots of a multi-grid simulation obtained by freezing the algorithm while the element, i (*highlighted in black*), of the first three grid levels (i.e., $l = 1, 2, 3$) is visited. *Arrows in subplot* **a** indicate the implemented scanning path. Colored cells are identified by index $j < i$ and have already been visited by the simulation path. White cells are identified by index $j > i$. The *red*, *green*, and *blue* elements in subplots **a**, **c**, and **e** belong respectively to the coarse, intermediate, and fine disjoint sets into which the domain is partitioned. The *colored blocks lying within the black squares* reside in the conditional neighborhood (Γ_i) of element i. The *orange and grey cells* in subplots **b**, **d**, and **f** indicate the diverse facies values assigned to each grid element during the simulation

The adoption of a MM model allows obtaining an explicit parameterization of the conditional probability expressed in Eq. 1. This is a key feature that will enable us to update the spatial distribution of the facies within each realization of the ensemble by conditioning the parameters of MM on available production data, as described in details in Section 3 (step 2).

Values of log permeabilities within each facies are described by a multi-Gaussian distribution with a given mean and spatial covariance function. Cross correlations between log permeabilities of different facies are assumed to be negligible.

3 Methodology

In this section, we describe our new data assimilation scheme for conditioning on available production data a collection of reservoirs characterized by random spatial distributions of geological facies and associated log permeabilities. For simplicity, we limit the illustration to the case where only two fluid phases (oil and water) are displaced in the host porous domain. The methodology can readily be extended to systems characterized by the simultaneous occurrence of three (or more) flowing fluid phases.

We consider the model vector

$$\psi = \begin{bmatrix} \mathbf{Y} \\ \mathbf{p} \\ \mathbf{S}_{wat} \\ \mathbf{w} \end{bmatrix} \tag{3}$$

Here $\mathbf{Y}$, $\mathbf{p}$, and $\mathbf{S}_{wat}$ are vectors containing static (e.g., log permeability, $\mathbf{Y}$) and dynamic (e.g., pressure, $\mathbf{p}$, and water saturation, $\mathbf{S}_{wat}$) variables at N_e numerical block centers, and the entries of vector $\mathbf{w}$ are N_w values of production data (e.g., fluid flow rates or bottom hole pressure values at well locations). Vector ψ is therefore of size $N_\psi = 3N_e + N_w$. We subdivide the time domain into a series of intervals delimited by the times at which measurements become available and focus on a generic time interval $\left(T_{k-1}\ T_k\right]$.

We introduce the vector $\psi^{u,T_{k-1}}$, where the superscript indicates that ψ is considered at time T_{k-1} and is conditioned on measurements available up to time T_{k-1}. The adoption of a Monte Carlo framework enables one to approximate the probability density function (pdf) of

$\psi^{u,T_{k-1}}$ by means of a collection of NMC equally likely model realizations of the system, defined as

$$\psi_j^{u,T_{k-1}} = \begin{bmatrix} \mathbf{Y} \\ \mathbf{p} \\ \mathbf{S}_{wat} \\ \mathbf{w} \end{bmatrix}_j^{u,T_{k-1}} \quad j = 1, \ldots, NMC \tag{4}$$

The corresponding forward vectors at time T_k are calculated as

$$\psi_j^{f,T_k} = \Phi\left(\psi_j^{u,T_{k-1}}\right) \quad j = 1, \ldots, NMC \tag{5}$$

thus enabling characterization of the pdf of ψ^{f,T_k} (i.e., here the superscript indicates that ψ is considered at time T_k and is conditioned on measurements available up to time T_{k-1}). The (generally nonlinear) operator Φ in Eq. 5 represents a multiphase flow model the solution of which is performed within time interval $\left(T_{k-1}\ T_k\right]$ by setting the log permeability field to $\mathbf{Y}_j^{u,T_{k-1}}$ $\left(i.e., \mathbf{Y}_j^{f,T_k} = \mathbf{Y}_j^{u,T_{k-1}}\right)$ and considering as initial conditions the pressure and water saturations equal to $\mathbf{p}_j^{u,T_{k-1}}$ and $\mathbf{S}_{wat,j}^{u,T_{k-1}}$, respectively. Boundary conditions for the flow simulation are here assumed to be deterministically known. We also note that terms included in vector $\mathbf{w}_j^{u,T_{k-1}}$ have no effect on the flow simulation.

We introduce the collection of vectors

$$\mathbf{s}_j^{f,T_k} \quad j = 1, ..., NMC \tag{6}$$

containing the facies identifiers at the N_e grid elements within the j-th realization at time T_k conditioned on measurements available up to time T_{k-1}, and the vectors

$$\mathbf{v}_j^{f,T_k} = \begin{bmatrix} \mathbf{s}^1 \\ \vdots \\ \mathbf{s}^K \end{bmatrix}_j^{f,T_k} \quad j = 1, \ldots, NMC \tag{7}$$

Here, each vector $\mathbf{s}_j^{k_f,f,T_k}$ of size N_e contains the indicator variables associated with facies $k_f = 1, ..., K$ within the j-th realization of the Monte Carlo collection.

The objective of the data assimilation algorithm is to calculate the updated vectors at time T_k, i.e., ψ_j^{u,T_k} and $\mathbf{s}_j^{u,T_k}$, conditioned on measured values of production data at time T_k, i.e., $\mathbf{w}^{T_k}$. Measurement errors can be considered upon randomly perturbing values of $\mathbf{w}^{T_k}$ and collecting them in vector $\mathbf{d}^{T_k}$ according to

$$\mathbf{d}^{T_k} = \mathbf{w}^{T_k} + \varepsilon^{T_k} \tag{8}$$

ε^{T_k} being a zero-mean Gaussian random vector with known covariance matrix $\mathbf{\Sigma}_{\varepsilon\varepsilon}^{T_k}$. To simplify the notation, in the following we will consider $\mathbf{\Sigma}_{\varepsilon\varepsilon}^{T_k}$ as a time-invariant quantity and will drop the superscript T_k.

The data assimilation scheme is developed through a four-step algorithm described in details in the following.

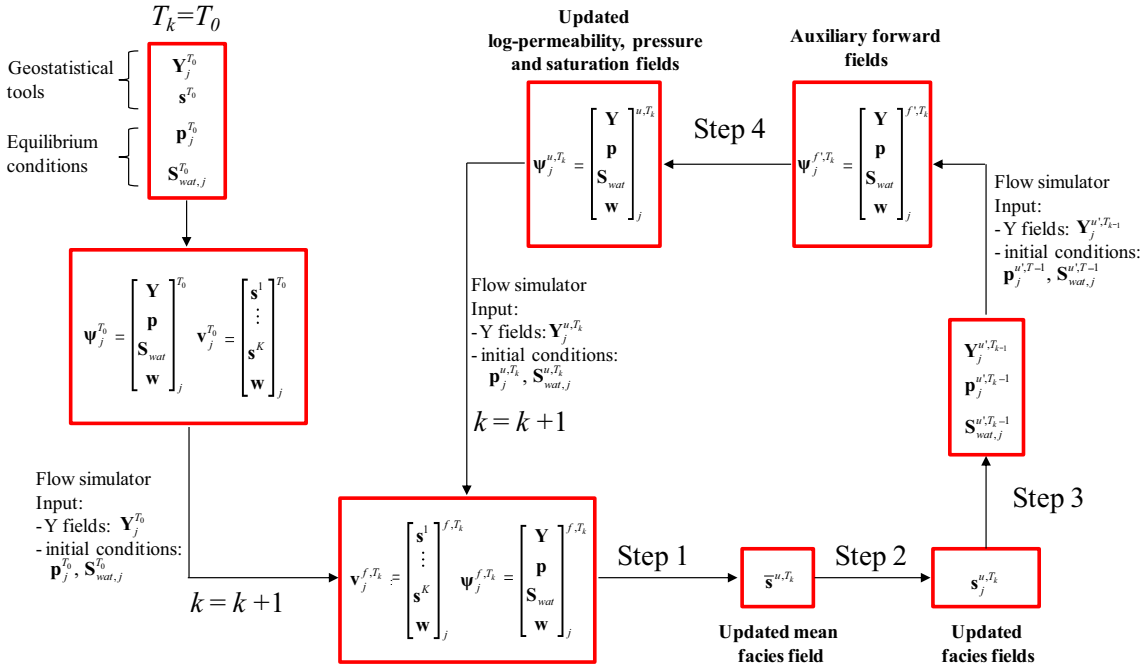

Fig. 2 Flow chart describing the proposed data assimilation algorithm

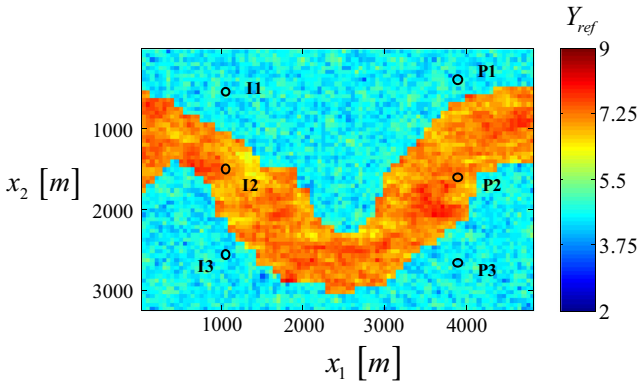

Fig. 3 Log permeability distribution (Y_{ref}) and well locations in the reference model. Injectors and producers are indicated as Ii and Pi ($i = 1, 2, 3$), respectively

Step 1: Updating the facies probability map

We start by considering the sample average of $\mathbf{v}_j^{f,T_k}$ defined in (7)

$$\overline{\mathbf{v}}^{f,T_k} = \frac{1}{NMC}\sum_{j=1}^{NMC}\mathbf{v}_j^{f,T_k} \tag{9}$$

Instead of updating each individual member of the collection, $\mathbf{v}_j^{f,T_k}$, as in the standard EnKF context, we evaluate the updated vector $\overline{\mathbf{v}}^{u,T_k}$ through the following averaged equation

$$\overline{\mathbf{v}}^{u,T_k} = \overline{\mathbf{v}}^{f,T_k} + \hat{\mathbf{\Sigma}}_{\mathbf{vw}}^{f,T_k}\left(\hat{\mathbf{\Sigma}}_{\mathbf{ww}}^{f,T_k} + \hat{\mathbf{\Sigma}}_{\varepsilon\varepsilon}\right)^{-1}\left(\overline{\mathbf{d}}^{T_k} - \overline{\mathbf{w}}^{f,T_k}\right) \tag{10}$$

Here, $\hat{\mathbf{\Sigma}}_{\mathbf{vw}}^{f,T_k}$ is the sample cross-covariance matrix between vectors $\mathbf{v}_j^{f,T_k}$ and $\mathbf{w}_j^{f,T_k}$; $\hat{\mathbf{\Sigma}}_{\mathbf{ww}}^{f,T_k}$ is the sample covariance matrix of vectors $\mathbf{w}_j^{f,T_k}$, while $\overline{\mathbf{d}}^{T_k}$ and $\hat{\mathbf{\Sigma}}_{\varepsilon\varepsilon}^{T_k}$ respectively are the sample mean and covariance matrix of the collection of randomized measurements $\mathbf{d}_j^{T_k} = \mathbf{d}^{T_k} + \varepsilon_j^{T_k}$. Note that the choice of updating the sample averages does not imply any assumption in addition to those associated with the update of individual replicates.

Step 2: Drawing a collection of updated facies field realizations

A new collection of facies realizations $\left(\mathbf{s}_j^{u,T_k},\ j = 1, ..., NMC\right)$ is generated via a Markov mesh (MM) model. This is accomplished by assuming that (a) the formulation of the MM model (i.e., number of parameters and size of the conditional neighborhood Γ) and (b) the functional form of the relationship expressing the conditional probability of observing a facies value over a grid element, i, given facies values over the conditional neighborhood, $\mathbf{s}_{\Gamma_i}$, coincide with those employed in an unconditional generation setting. The only components of the MM model updated in this step are then the values of the parameters contained in vectors $\theta_{l(i)}^{k_f}$, $k_f = 1, ..., K; l(i) = 1, ..., L$. After conditioning on the dynamic data, MM will be no longer stationary in space. For this reason, we let the updated values of MM parameters to vary with the element index, i. This is achieved by visiting each element of the grid according to the sequential path defined for the MM model. A new facies identifier is assigned to element i visited by the algorithm in each updated grid j of the collection $\left(s_{i,j}^{u,T_k}\right)$ according to the conditional probability

$$\pi\left(s_{i,j}^{u,T_k}\middle|\mathbf{s}_{\Gamma_i,j}^{u,T_k}\right) = \frac{\prod_{k_f=1}^{K}\exp\left\{s_{i,j}^{k_f,u,T_k}\mathbf{z}_{i,j}^{+}\left(\theta_{l(i)}^{k_f} + \boldsymbol{\lambda}_i^{k_f}\right)\right\}}{\sum_{k_f=1}^{K}\exp\left\{\mathbf{z}_{i,j}^{+}\left(\theta_{l(i)}^{k_f} + \boldsymbol{\lambda}_i^{k_f}\right)\right\}} \quad j = 1, ..., NMC \tag{11}$$

Relying on Eq. 11 ensures that the mean facies distribution $\left(\overline{\mathbf{v}}^{u,T_k}\right)$ obtained at step 1 is honored. The values of the unknown vectors $\boldsymbol{\lambda}_i^{k_f}$ in Eq. 11 are tuned to satisfy

$$\frac{1}{NMC}\sum_{j=1}^{NMC}s_{i,j}^{k_f,u,T_k} = \bar{s}_i^{k_f,u,T_k} \quad k_f = 1, ..., NMC \tag{12}$$

The term appearing on the right hand side of Eq. 12 is an element of the vector updated through (10). One can note that Eq. 11 reduces to Eq. 1 when all components of $\boldsymbol{\lambda}_i^{k_f}$ vanish. In practice, Eqs. 11–12 are used to update the probability of the MM, $\pi\left(s_i\middle|\mathbf{s}_{\Gamma_i}\right)$, which is not conditioned on the production data, to the probability $\pi\left(s_i^{u,T_k}\middle|\mathbf{s}_{\Gamma_i}^{u,T_k}\right)$, conditioned on the information provided by the measurements available up to time T_k. In our implementation, we consider all elements of $\boldsymbol{\lambda}_i^{k_f}$

Table 1 Parameters adopted for the generation of the reference log permeability field

	Mean*	Sill	Nugget	Range along x_1 (m)	Range along x_2 (m)
Facies 1	7.1	0.10	0.0	500.0	250.0
Facies 2	4.6	0.10	0.0	100.0	100.0

*Permeability values are expressed in millidarcy

equal to zero with the exception of its last entry. The latter is set to the unknown scalar $\lambda_i^{k_f}$, which depends on the lithofacies type. This strategy ensures that the conditional probability (11) be a monotonic function of $\lambda_i^{k_f}$. The estimation of $\lambda_i^{k_f}$ can then be readily accomplished through a bisection algorithm. Our numerical results show that this simple strategy yields results of remarkable quality, in the sense that the updated spatial distribution of facies maintains spatial correlations which are quantitatively similar to those observed before the assimilation of production data. Functional forms of $\boldsymbol{\lambda}_i^{k_f}$ with increased complexity and different algorithms for its estimation can be accommodated in the procedure.

Step 3: Ensuring consistency between the updated facies fields and the underlying petrophysical properties

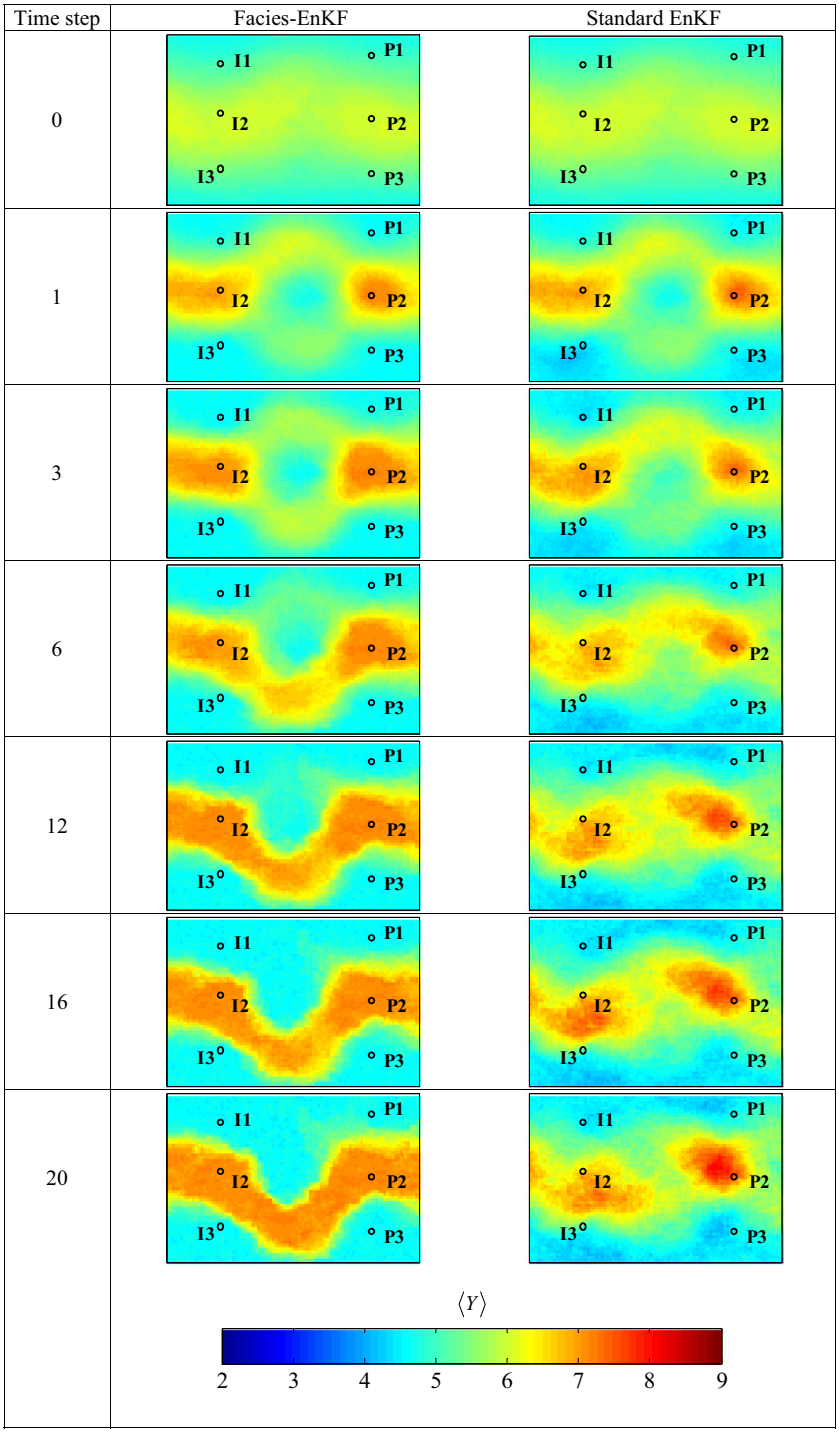

Fig. 4 Estimates of mean log permeability at initial time and at six selected assimilation steps obtained through Facies-EnKF and standard EnKF

We recall that up to this point, we have evaluated the vectors $\mathbf{s}_j^{u,T_k}$ and $j = 1, ..., NMC$, which are the realizations of the facies fields conditioned on the measurements available up to time T_k. Before updating the vectors of model realizations, ψ_j^{f,T_k}, we solve the flow problem within the time interval $\left(T_{k-1}\ T_k\right]$ upon replacing the model parameters and the system states updated at time T_{k-1} $\left(i.e., \mathbf{Y}_j^{u,T_{k-1}}, \mathbf{p}_j^{u,T_{k-1}}, \text{and } \mathbf{S}_{wat,j}^{u,T_{k-1}}\right)$ through the corresponding auxiliary fields $\left(\mathbf{Y}_j^{u',T_{k-1}}, \mathbf{p}_j^{u',T_{k-1}}, \text{and } \mathbf{S}_{wat,j}^{u',T_{k-1}}\right)$ to ensure consistency with the underlying facies fields updated through steps 1–2. We do so by expressing the auxiliary log permeability and pressure/saturation fields, i.e., $\mathbf{Y}_j^{u',T_{k-1}}$, $\mathbf{p}_j^{u',T_{k-1}}$, and $\mathbf{S}_{wat,j}^{u',T_{k-1}}$, as a linear transformation of $\mathbf{Y}_j^{u,T_{k-1}}$, $\mathbf{p}_j^{u,T_{k-1}}$, and $\mathbf{S}_{wat,j}^{u,T_{k-1}}$, thus preserving the ensemble statistics (mean and covariance) of the latter.

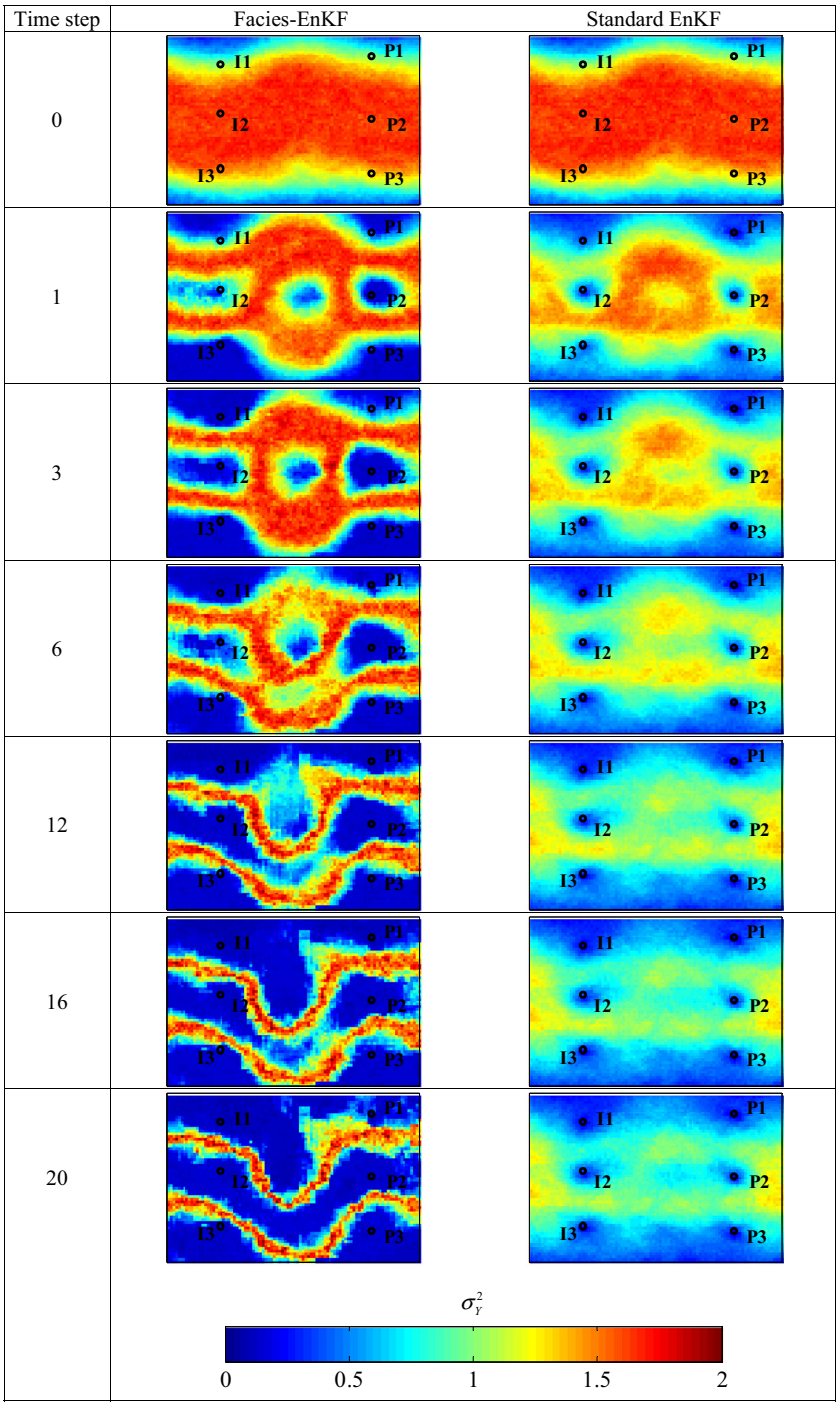

Fig. 5 Estimation variance of log permeability at initial time and at six selected assimilation steps obtained through Facies-EnKF and standard EnKF

Each auxiliary updated realization is then used as input vector in the flow simulator (5) to obtain the auxiliary forward vectors at time T_k, ψ_j^{f',T_k}. These will be further conditioned on the measurements available at time T_k during step 4. In practice, one can note that the additional flow simulation performed at step 3 allows alleviating the appearance of unphysical updates in the model state vectors.

Step 4: Updating the petrophysical properties

We propose to evaluate the updated state vectors $\psi_j^{u,T}$ at time T_k through

$$\psi_j^{u,T_k} = \psi_j^{f',T_k} + \hat{\mathbf{\Sigma}}_{\psi\mathbf{w},j}^{f',T_k}\left(\hat{\mathbf{\Sigma}}_{\mathbf{ww}}^{f',T_k} + \hat{\mathbf{\Sigma}}_{\varepsilon\varepsilon}\right)^{-1}\left(\mathbf{d}_j^{T_k} - \mathbf{w}_j^{f',T_k}\right) \quad j = 1,\ldots,NMC \tag{13}$$

Here, $\hat{\mathbf{\Sigma}}_{\psi\mathbf{w},j}^{f',T_k}$ is the sample cross-covariance matrix between vectors ψ_j^{f',T_k} and $\mathbf{w}_j^{f',T_k}$. In contrast with the standard EnKF scheme, where the sample cross-covariance between the production datum n and the model variable m associated with a given block m^* in the reservoir is evaluated on the basis of all the ensemble members, we compute it by considering only the members of the collection where the same facies value of the element m^* considered in the target model realization, j, occurs. This strategy is adopted because the scatter plots between petrophysical parameters (or system state variables) and production data of a reservoir model characterized by distinct (and randomly distributed) facies are typically arranged in clusters, each associated with a particular facies identifier.

Figure 2 provides a graphical depiction of the data assimilation algorithm described through steps 1–4.

4 Synthetic example

Here, we explore the applicability and accuracy of the data assimilation scheme described in Section 3 by way of a synthetic example. We consider a flow domain of size

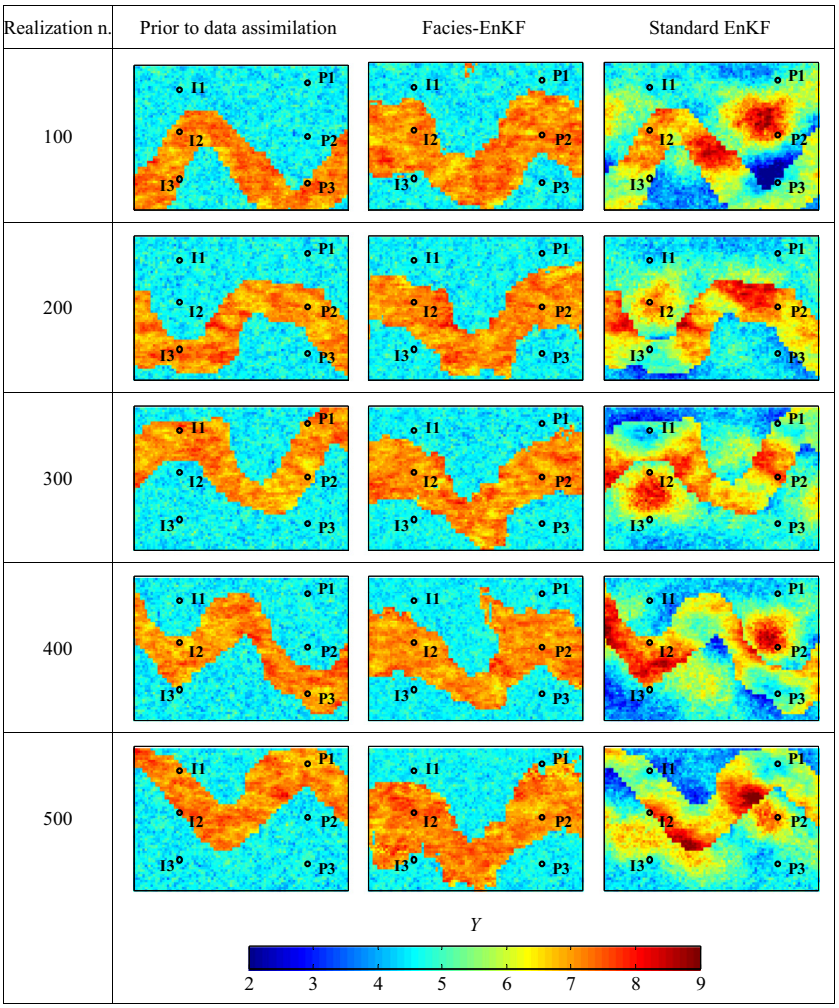

Fig. 6 Five selected realizations of the log permeability field generated before starting data assimilation and updated after the latest assimilation step with Facies-EnKF and standard EnKF

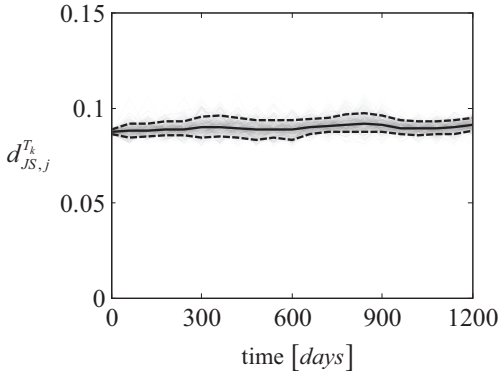

Fig. 7 Time dependence of the distances between multiple-point histograms (MPH) of each facies realization updated through Facies-EnKF and MPH of the training image (*solid grey curves*) evaluated in terms of the Jensen-Shannon divergence. The corresponding mean (*solid black line*) and 10th and 90th percentile (*dashed black line*) are also depicted

4800 m × 3200 m × 5 m along directions x_1, x_2, and x_3 (x_3 being vertical direction), respectively. The domain is discretized into grid cells of uniform size of 50 m × 50 m × 5 m (i.e., 96 × 64 × 1 blocks, yielding $N_e = 6144$). The reference model of the reservoir is formed by two facies (i.e., $K = 2$) whose spatial distribution is obtained by the MM model with characteristic parameters estimated from a training image characterized by the presence of meandering channels. Our implementation of the multi-grid MM model is based on a sequential path which starts from the left bottom corner of the grid and proceeds along a sequence of diagonal directions to scan the entire domain. We employ four grid levels and an isotropic refinement scheme similar to the one depicted in Fig. 1. We adopt a squared conditional neighborhood, Γ, of size equal to 21 for the coarsest grid level; the size of Γ then decreases to 7, 7, and 5 with increasing order of grid level refinement. The computational time required for the estimation of the MM parameters is approximately 13 min on a 2.80-GHz Intel i7-860 processor. Simulation of a single unconditional facies field requires about 4 s.

The domain is then populated with the corresponding petrophysical properties (i.e., the log permeability), yielding the reference field depicted in Fig. 3. Log permeabilities are generated at element centers using a sequential Gaussian simulator, with exponential covariance function and statistical parameters listed in Table 1. The porosity field is assumed to be a deterministic constant equal to 0.2, yielding a global pore volume of 15.36×10^6 m^3.

We simulate transient flow for a time period of 1200 days driven by six wells operating in the domain of interest. Three wells (P1, P2, and P3) are producers and work at a

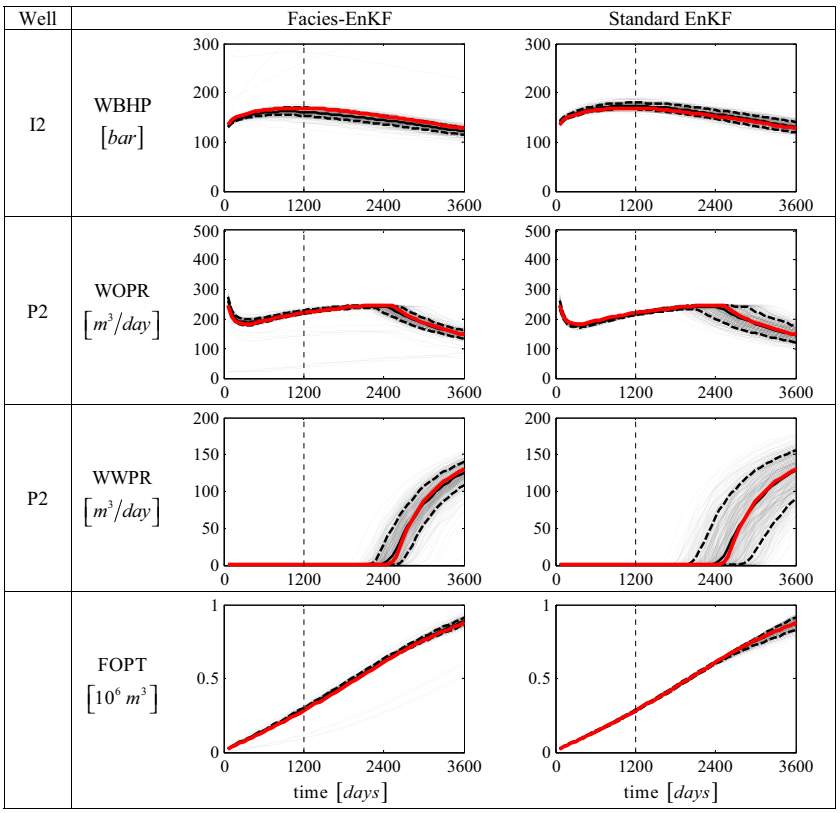

Fig. 8 Temporal dynamics of estimated production values at wells I2 and P2 and FOPT values for the collection of models updated through Facies-EnKF and standard EnKF (*solid grey line*) during TS1. Corresponding mean (*solid black line*) and 10th and 90th percentile (*dashed black line*) are also depicted. *Red curves* correspond to the reference model solution. *Vertical dashed lines* separate the assimilation period from the forecast period

fixed bottom hole pressure (BHP) equal to 30 bar. The three wells I1, I2, and I3 inject water at constant rates of 30, 230, and 30 m^3 day^{-1}, respectively. As shown in Fig. 3, only wells I2 and P2 lie in the region of the domain characterized by the highest permeability path. A uniform initial oil saturation of 0.8 is imposed on the system. The initial pressure is set to a uniform value of 100 bar while all external domain boundaries are impervious. We sample the reference production curves at 20 observation times, each separated by a fixed lag of 60 days (i.e., T_k =60, 120,... 1200 days), and perturb these by white Gaussian noises having standard deviations $\sigma_\varepsilon = 5$ m^3 day^{-1} and 5 bar for flow rates and pressures, respectively, reflecting measurement errors. In this setting, $\mathbf{\Sigma}_{\varepsilon\varepsilon}^{T_k}$ is a time-independent diagonal matrix with diagonal elements all equal to σ_ε^2.

We generate the initial collection of model realizations by assuming a perfect knowledge of the statistical models describing the spatial distribution of the geological and of the petrophysical properties within the domain of interest. This allows testing the robustness and accuracy of the

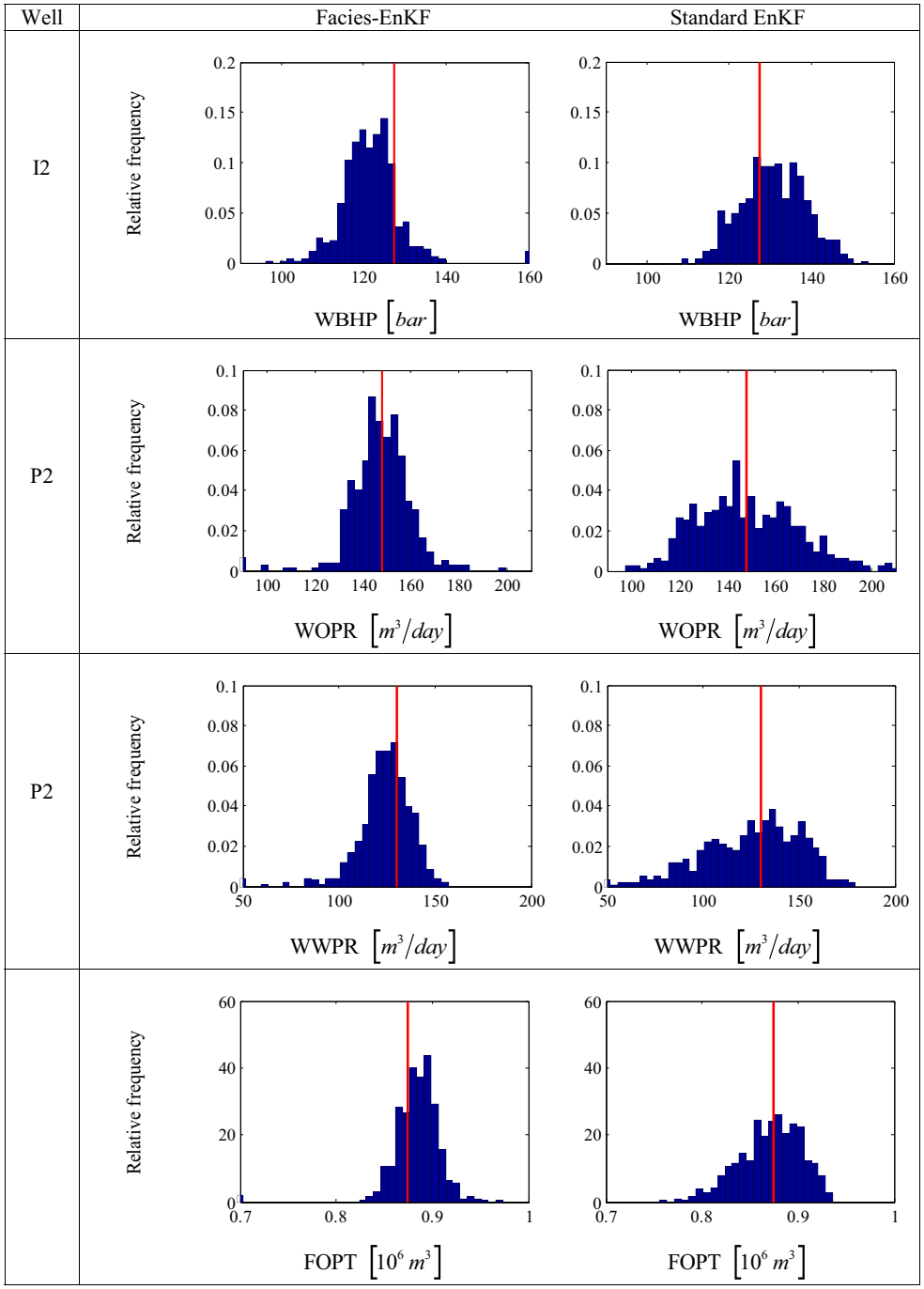

Fig. 9 Histograms of estimated production values at wells I2 and P2 and FOPT values at time 3600 days for TS1. *Vertical red lines* indicate corresponding reference values

proposed algorithm without introducing additional sources of uncertainty in our analysis. We generate a collection of 500 (i.e., $NMC = 500$) spatial fields of facies through the MM model by using the same parameters employed for the construction of the reference field. Then, each facies realization is populated by log permeability values evaluated by a sequential Gaussian simulator and adopting the same variogram functions and parameters used for the generation of the reference field.

We analyze the performance and accuracy of the proposed inversion algorithm (denoted in the following as Facies-EnKF) and compare it against the results obtained through the standard EnKF (e.g., [6, 12]. The latter allows updating the model state vectors defined in Eq. 4 at each assimilation step T_k through

$$\psi_j^{u,T_k} = \psi_j^{f,T_k} + \hat{\mathbf{\Sigma}}_{\psi\mathbf{w}}^{f,T_k}\left(\hat{\mathbf{\Sigma}}_{\mathbf{ww}}^{f,T_k} + \hat{\mathbf{\Sigma}}_{\varepsilon\varepsilon}^{T_k}\right)^{-1}\left(\mathbf{d}_j^{T_k} - \mathbf{w}_j^{f,T_k}\right) \quad j = 1, ..., NMC \tag{14}$$

where $\hat{\mathbf{\Sigma}}_{\psi\mathbf{w}}^{f,T_k}$ is the sample cross-covariance matrix between vectors ψ_j^{f,T_k} and $\mathbf{w}_j^{f,T_k}$, while $\hat{\mathbf{\Sigma}}_{\mathbf{ww}}^{f,T_k}$ is the sample covariance matrix of $\mathbf{w}_j^{f,T_k}$.

We start the assimilation with the same collection of model realizations for Facies-EnKF and its standard application counterpart. For the latter, we also investigate the benefits of localizing the cross-covariance matrix through the Gaspari-Cohn tapering function [13] to dampen the update of the system variables that are located too far from the observation points. In our tests, we did not observe any significant improvement in the quality of the calibration and in the prediction ability of the model realizations updated through the use of a covariance localization technique (not shown). For this reason, we focus in the following only on the results obtained without application of any localization techniques.

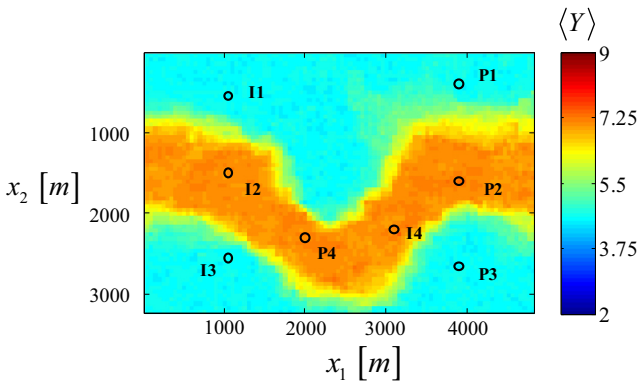

Fig. 10 Spatial location of wells I4 and P4 employed in TS2 and the mean log permeability distribution estimated through Facies-EnKF after the latest assimilation step

Figures 4 and 5 respectively show the spatial distribution of mean and variance of the initial and updated log permeability fields at six selected assimilation steps computed using Facies-EnKF and standard EnKF. During the earliest assimilation steps, the estimated mean fields obtained with the two approaches are similar and suggest the possibility that high-permeability inclusions associated with meandering channels occurs both within the upper and the lower parts of the domain. Assimilation of additional data in the model is conducive to estimates of log permeability obtained with Facies-EnKF that evolve toward a spatial pattern which is similar to that of the reference field and enables one to properly identify the location of the channelized region associated with the highest permeability values. It can be noted that the sampled bottom hole pressure curves of injectors I1 and I3 play a key role for an appropriate facies identification because these two wells inject water at the same flow rate but are associated with slightly different bottom hole pressure values. We can then deduce that I1 is characterized by lower injectivity and should be located farther from the high permeable channel. The estimated variance field obtained through Facies-EnKF after the latest assimilation step suggests that the calibrated values of Y are characterized by highest uncertainty within regions located in the proximity of the internal boundary demarcating the two geological facies. These results are not mirrored by the fields calibrated through standard EnKF. In these fields, the regions associated with the highest estimated permeabilities correspond only in part to the high permeable pattern displayed in the reference field. Figure 4 shows that the standard EnKF algorithm identifies correctly the presence of high/low permeable regions around each well but is not able to capture the global internal architecture of the system. From a general standpoint, this result is consistent with the observation that EnKF performs optimally only in multi-Gaussian fields. Therefore, our observations also contribute to highlight the known limitations of standard EnKF in applications involving the need to consider explicitly the occurrence of diverse geological facies. Taking this aspect into account corresponds to conceptualizing the system as a composite medium (e.g., [29, 37] and references therein) where the reservoir is modeled as a doubly stochastic process, i.e., randomness is associated with spatial distribution of facies as well as attributes within each facies.

Figure 6 depicts five selected realizations of log permeability generated prior to data assimilation and updated after the latest assimilation step using the two analyzed methodologies. These results evidence that the realizations calibrated through standard EnKF do not preserve the correct geological architecture, as opposed to fields estimated through our proposed method, which is consistent with the composite nature of the domain. Visual inspection of Fig. 6

suggests that the fields updated through Facies-EnKF tend to display a degree of spatial variability of log permeabilities which is similar to the one characterizing the reference model.

We quantify these observed behaviors through the concept of multiple-point histogram (MPH) [9]. We perform this analysis by choosing a template of size 4 × 4 grid elements and by considering all possible facies configurations that can occur within this template. An index is assigned to each facies configuration, and MPH associated with a given facies field is built by calculating the frequencies with which each configuration is reproduced in the considered field. We follow [33] and use the Jensen-Shannon divergence [11] to calculate the distance, $d_{JS,j}^{T_k}$, between the MPH of each updated facies realization, $MPH_j^{T_k}$, and MPH of the training image, MPH^{TI}. Figure 7 depicts the time dependence of $d_{JS,j}^{T_k}$ evaluated for all facies realizations updated through Facies-EnKF. These

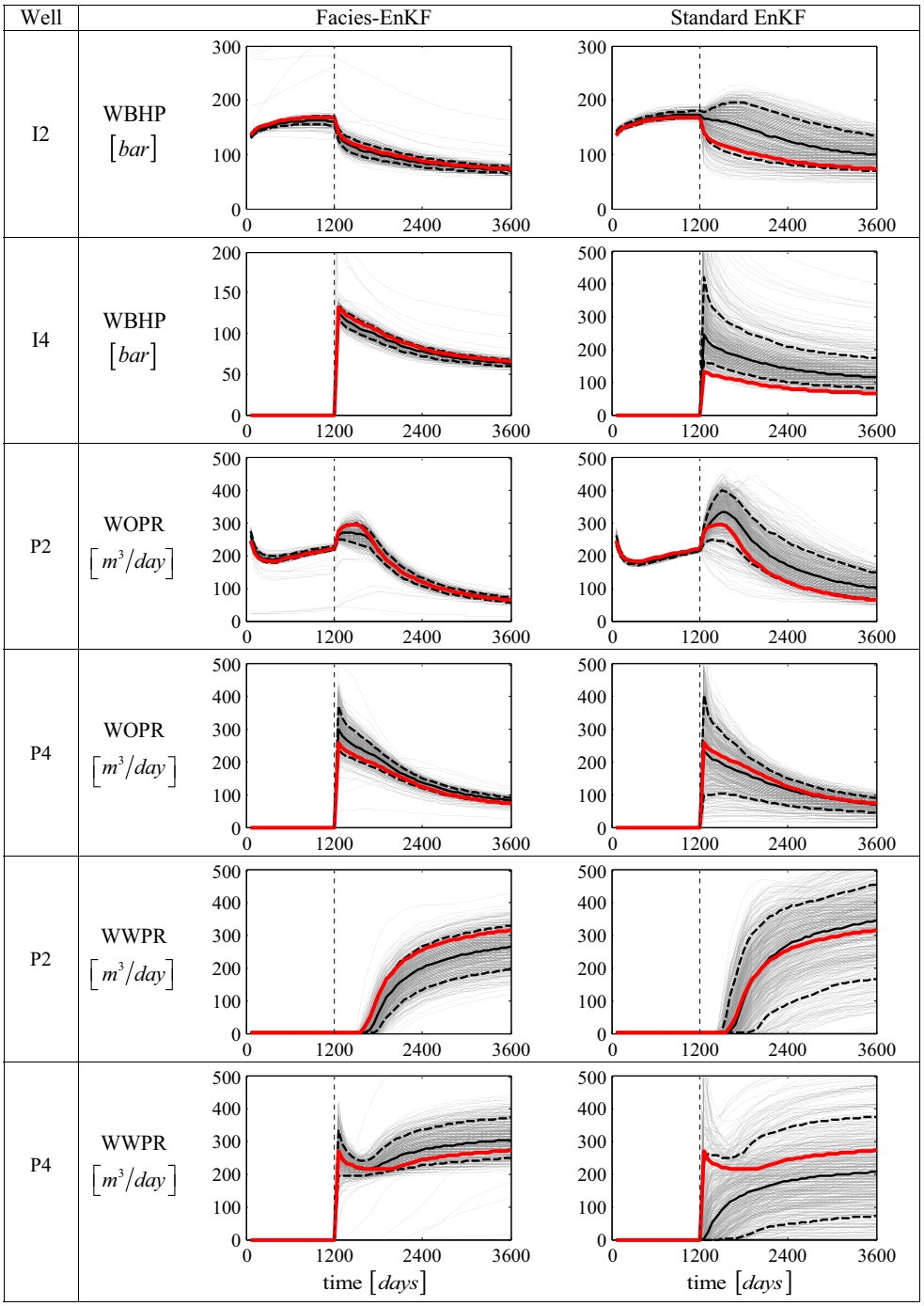

Fig. 11 Temporal dynamics of estimated production values at wells I2, I4, P2, and P4 for the collection of models updated employing Facies-EnKF and standard EnKF (*solid grey line*) during TS2. Corresponding mean (*solid black line*) and 10th and 90th percentile (*dashed black line*) are also depicted. *Red curves* correspond to the reference model solution. *Vertical dashed lines* separate the assimilation period from the forecast period

results provide quantitative confirmation that each updated facies realization is associated with a spatial arrangement of facies consistent with the key pattern characterizing the training image.

We analyze the ability of the updated model realizations to predict production dynamics during a forecast window of 2400 days after the latest assimilation time. This analysis is performed by rerunning the flow simulation for all calibrated log permeability fields from the initial time $T_0 = 0$ and for a total simulation period of 3600 days. We explore two distinct scenarios differing from each other in the flow configuration imposed during the target additional time window. In our first test scenario, denoted as TS1, the same flow setting considered during the assimilation period is projected onto the future scenario evaluation. A second study (denoted as TS2) is performed by considering the presence of two additional wells (i.e., a producer and an injector) that become operative after $T_{20} = 1200$ days.

Figure 8 depicts the collection of curves obtained for TS1 through Facies-EnKF and EnKF and describing bottom hole pressure dynamics (WBHP) at injector I2, the production rates of oil (WOPR) and water (WWPR) at P2, and the field oil production (FOPT). Predicted and reference bottom hole pressures at wells I1 and I3 and oil flow rates at wells P1 and P3 display trends that are qualitatively similar to those related to wells I2 and P2, respectively, and are not shown. Figure 8 shows that the predicted pressure curves and oil/water production rates obtained from the two sets of calibrated fields are in good agreement with the corresponding reference production curves (which have been obtained upon relying on the true, reference reservoir model). The model realizations calibrated through standard EnKF provide a remarkably high-quality prediction despite the observation that the corresponding log permeability distributions do not honor the correct geology architecture of the reference reservoir (see Figs. 4–6). We also note that oil and water flow rates at well P2 predicted through Facies-EnKF are characterized by an overall uncertainty which is smaller than that associated with the corresponding estimates based on standard EnKF. It is striking that realizations updated through Facies-EnKF can provide a notably accurate prediction (with a relative small prediction

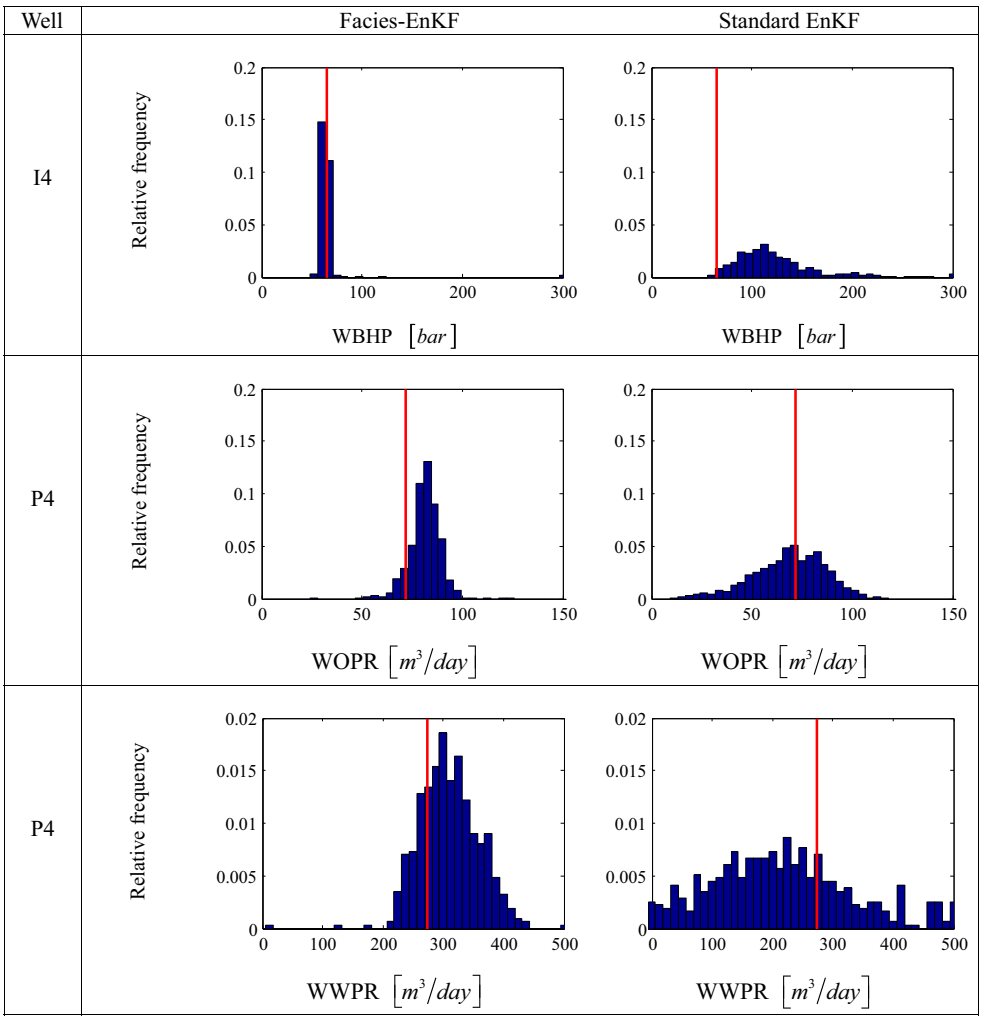

Fig. 12 Histograms of estimated production values at wells I4 and P4 at time 3600 days for TS2. *Vertical red lines* indicate corresponding reference values

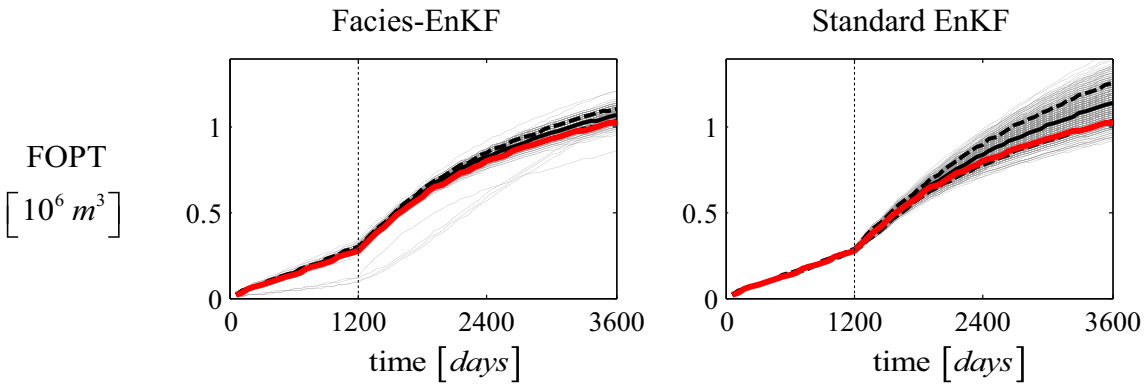

Fig. 13 Time dependence of FOPT for the collection of models updated through Facies-EnKF and standard EnKF (*solid grey line*) during TS2. Corresponding mean (*solid black line*) and 10th and 90th percentile (*dashed black line*) are also depicted. *Red curves* correspond to the reference model solution. *Vertical dashed lines* separate the assimilation period from the forecast period

error) of the water breakthrough at well P2, even as the first water breakthrough time at this well in the reference model occurs after the assimilation period, approximately at time $T^* = 2400$ days.

Figure 9 compares Facies-EnKF and standard EnKF-based sample histograms of the predicted bottom hole pressures at well I2, WOPR and WWPR at well P2, as well as FOPT at the final simulation time (i.e., 3600 days). While both data assimilation approaches yield a relatively good agreement between the estimated curves and the reference pressure and production history (see Fig. 8), predictions obtained through standard EnKF are characterized by the largest uncertainty, as can be seen from the degree of spreading of the histograms.

In TS2, we explore the scenario associated with the presence of two additional wells (i.e., injector I4 and producer P4) starting their operation after time $T_{20} = 1200$ days. The locations of these new wells are depicted in Fig. 10 and are selected upon relying on the information provided by the mean log permeability field updated through Facies-EnKF, which displays in these positions a large probability of occurrence of the high-permeability facies. Wells I4 and P4 are set to function at a fixed water flow rate of 450 $m^3\ s^{-1}$ and at a constant bottom hole pressure of 30 bar, respectively.

Figures 11 and 12 depict the production curves at wells I2, I4, P2, and P4 predicted through the model realizations updated with the two assimilation approaches. These figures evidence the improved prediction ability of the collection of reservoirs updated through Facies-EnKF with respect to the one calibrated via standard EnKF. All production curves estimated through Facies-EnKF provide a remarkably improved agreement with the reference production values and are characterized by a significantly smaller degree of uncertainty than those obtained through standard EnKF. The increased prediction ability of the model realizations updated through Facies-EnKF leads to a markedly precise estimation of the total oil production curve, FOPT, as shown in Figs. 13 and 14.

We conclude our analysis by comparing the computational costs of the two approaches. A single assimilation step on a 2.80-GHz Intel i7-860 processor requires 3400 and 8500 s, respectively, for standard EnKF and Facies-EnKF. Our proposed algorithm requires more CPU time

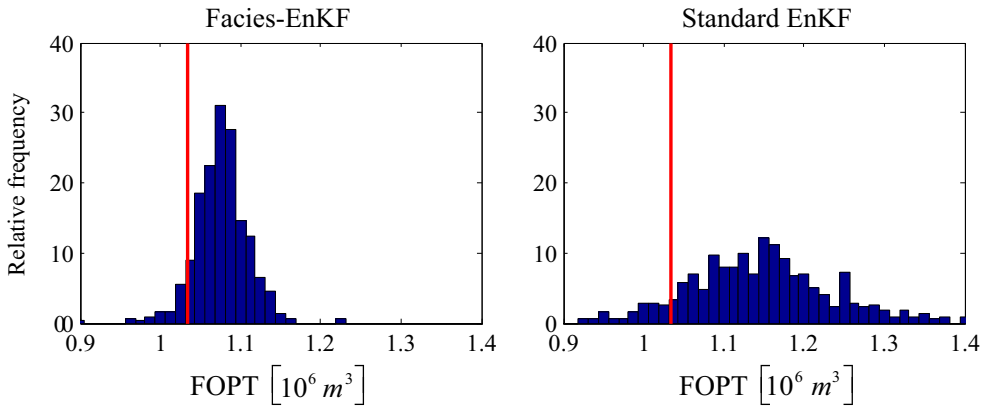

Fig. 14 Histograms of FOPT values predicted at time 3600 days for TS2. *Vertical red lines* indicate corresponding reference values

than does standard EnKF because (a) the flow simulations are iterated and must be performed twice within each updating step and (b) the facies fields must be regenerated at each assimilation time. However, one can note that the increase of CPU time is not dramatic and the use of Facies-EnKF is fully justified by the consistency of the approach with the composite nature of the domain which leads to a significantly improved prediction ability of the updated model realizations.

5 Conclusions

We present and discuss a novel data assimilation algorithm conducive to conditioning the spatial distribution of the geological and petrophysical properties of a collection of reservoir model realizations characterized by a complex geological architecture on available production data collected in the field. The approach is fully consistent with modern interpretive concepts depicting a porous formation as a composite medium where the distribution of both geomaterials/facies and associated attributes is modeled as stochastic processes of space.

The proposed algorithm relies on a Markov mesh (MM) model to describe the uncertain spatial distribution of the facies in the domain of interest. We integrate the MM within a data assimilation scheme based on the ensemble Kalman filter (EnKF) approach. The methodology is analyzed and tested against standard EnKF by means of a synthetic study where the reference model of the reservoir is characterized by the presence of two distinct facies representing a complex meandering high-permeability channel embedded in a lower permeability background matrix. We show that our scheme allows obtaining a set of conditional realizations for which the spatial distribution of facies and log permeabilities is consistent with prior information on the internal architecture of the target system. We investigate the ability of the model realizations calibrated through the analyzed approaches to correctly predict future behavior of the reference reservoir model. This analysis is performed by considering two plausible scenarios, according to which diverse flow configurations are imposed after the assimilation period. The results suggest that the model realizations calibrated by means of the standard EnKF provide acceptable estimates of the system future performances only when the flow configuration acting during the assimilation and forecast is identical. Otherwise, a very poor quality prediction is obtained. Model realizations updated through our Facies-EnKF provide a remarkably accurate prediction of future reservoir production dynamics for all analyzed scenarios. These estimations are characterized by a smaller degree of uncertainty when compared to those obtained through the standard EnKF. From an operational standpoint, the use of Facies-EnKF, even in the presence of a modest increase of CPU time when compared to standard EnKF, is fully justified by the consistency of the approach with the composite nature of the domain which leads to a significantly improved prediction ability of the updated model realizations.

A critical issue of the synthetic study analyzed here is related to the assumption that the statistical models describing the spatial distribution of the geological and petrophysical properties are known without uncertainty. Prior knowledge about the geological architecture of a reservoir could be represented by multiple and equally plausible conceptual scenarios. One way to rigorously address this issue would be to employ a multi-model approach of the kind proposed by, e.g., [20], with which our data assimilation methodology is fully compatible. A complete and rigorous integration of a multi-model approach within our data assimilation framework could be part of a further study. Further developments of our work include also the characterization of reservoir models characterized by the occurrence of multiple geological units.

Acknowledgments We thank Eni S.p.A. for the permission to publish this paper. Schlumberger is acknowledged for allowing the use of the software ECLIPSE for research purposes.

References

1. Aanonsen, S.I., Nævdal, G., Oliver, D.S., Reynolds, A.C., Vallès, B.: The ensemble Kalman filter in reservoir engineering—a review. SPE J. **14**(3), 393–412 (2009). doi:10.2118/117274-PA
2. Abend, K., Harley, T.J., Kanal, L.N.: Classification of binary random patterns. IEEE Trans. Inf. Theory **11**(4), 538–544 (1965). doi:10.1109/TIT.1965.1053827
3. Arpat, G.B., Caers, J.: Conditional simulation with patterns. Math. Geol **39**(2), 177–203 (2007). doi:10.1007/s11004-006-9075-3
4. Astrakova, A., Oliver, D.S.: Conditioning truncated pluri-Gaussian models to facies observations in ensemble-Kalman-based data assimilation. Math. Geosci. **47**(3), 345–367 (2014). doi:10.1007/s11004-014-9532-3
5. Bridge, J.S., Leeder, M.R.: A simulation model of alluvial stratigraphy. Sedimentology **26**(5), 617–644 (1979). doi:10.1111/j.1365-3091.1979.tb00935.x
6. Burgers, G., van Leeuwen, P.J., Evensen, G.: Analysis scheme in the ensemble Kalman filter. Mon. Weather Rev. **126**(6), 1719–1724 (1998). doi:10.1175/1520-0493(1998)126<1719:ASITEK>2.0.CO;2
7. Daly, C.: Higher order models using entropy, Markov random fields and sequential simulation. In: Leuangthong, O., Deutsch, C.V. (eds.) Geostatistics Banff, pp. 215–224. Springer, Berlin (2005)
8. Deutsch, C.V., Wang, L.: Hierarchical object-based stochastic modeling of fluvial reservoirs. Math. Geol. **28**(7), 857–880 (1996). doi:10.1007/BF02066005
9. Deutsch, C.V., Gringarten, E.: Accounting for multiple-point continuity in geostatistical modeling, p. 2000. Geostatistical Congress, South Africa (2000)

10. Deutsch, C.V., Tran, T.T.: FLUVSIM: a program for object-based stochastic modeling of fluvial depositional systems. Comput. Geosci. **28**(4), 525–535 (2002). doi:10.1016/S0098-3004(01)00075-9
11. Endres, D.M., Schindelin, J.E.: A new metric for probability distributions. IEEE Trans. Inf. Theory **49**(7), 1858–1860 (2003). doi:10.1109/TIT.2003.813506
12. Evensen, G.: Sequential data assimilation with a nonlinear quasi-geostrophic model using Monte Carlo methods to forecast error statistics. J. Geophys. Res. **99**(C5), 10143–10162 (1994). doi:10.1029/94JC00572
13. Gaspari, G., Cohn, S.E.: Construction of correlation functions in two and three dimensions. Q. J. R. Meteorol. Soc **125**(554), 723–757 (1999). doi:10.1002/qj.49712555417
14. Gross, L.J., Small, M.J.: River and floodplain process simulation for subsurface characterization. Water Resour. Res. **34**(9), 2365–2376 (1998). doi:10.1029/98WR00777
15. Hu, L.Y., Zhao, Y., Liu, Y., Scheepens, C., Bouchard, A.: Updating multipoint simulations using the ensemble Kalman filter. Comput. Geosci. **51**, 7–15 (2013). doi:10.1016/j.cageo.2012.08.020
16. Jafarpour, B., McLaughlin, D.B.: History matching with an ensemble Kalman filter and discrete cosine parameterization. Comput. Geosci. **12**(2), 227–244 (2008). doi:10.1007/s10596-008-9080-3
17. Jafarpour, B., Khodabakhshi, M.: A probability conditioning method (PCM) for nonlinear flow data integration into multipoint statistical facies simulation. Math. Geosci. **43**(2), 133–164 (2011). doi:10.1007/s11004-011-9316-y
18. Journel, A.G.: Combining knowledge from diverse sources: an alternative to traditional data independence hypotheses. Math. Geol. **34**(5), 573-596 (2002). doi:10.1023/A:1016047012594
19. Kjønsberg, H., Kolbjørnsen, O.: Markov mesh simulations with data conditioning through indicator kriging. In: Proceedings of the eighth international geostatistics congress, vol. 1, pp. 257–266. Kluwer, Dordrecht (2008)
20. Khodabakhshi, M., Jafarpour, B.: A Bayesian mixture-modeling approach for flow-conditioned multiple-point statistical facies simulation from uncertain training images. Water Resour. Res. **49**(1), 328–342 (2013). doi:10.1029/2011WR010787
21. Kolbjørnsen, O., Stien, M., Kjønsberg, H., Fjellvoll, B., Abrahamsen, P.: Using multiple grids in Markov mesh facies modeling. Math. Geosci. **46**(2), 205–225 (2014). doi:10.1007/s11004-013-9499-5
22. Le Loc'h, G., Galli, A.: Truncated plurigaussian method: theoretical and practical points of view. In: Baafi, E.Y., Schofield, N.A. (eds.) Geostatistics Wollongong 96, pp. 211222. Kluwer Academic Press, Dordrecht (1997)
23. Liu, N., Oliver, D.S.: Ensemble Kalman filter for automatic history matching of geologic facies. J. Petrol. Sci. Eng **47**(3-4), 147–161 (2005). doi:10.1016/j.petrol.2005.03.006
24. Liu, N., Oliver, D.S.: Critical evaluation of the ensemble Kalman filter on history matching of geologic facies. SPE Reserv. Eval. Eng. **8**(6), 470–477 (2005). doi:10.2118/92867-PA
25. Matheron, G., Beucher, H., de Fouquet, C., Galli, A., Guerillot, D., Ravenne, C.: Conditional simulation of the geometry of fluvio-deltaic reservoirs. In: SPE Annual Technical Conference and Exhibition, 27-30 September, Dallas, pp. 123–131 (1987). doi:10.2118/16753-MS
26. Moreno, D., Aanonsen, S.I.: Stochastic facies modeling using the level set method. In: Petroleum Geostatistics, 10–14 September 2007, Cascais, Portugal, A16, Extended Abstracts Book, EAGE Publications BV, Utrecht (2007)
27. Oliver, D.S., Chen, Y.: Recent progress on reservoir history matching: a review. Comput. Geosci. **15**(1), 185–221 (2011). doi:10.1007/s10596-010-9194-2
28. Oliver, D.S., Chen, Y., Nævdal, G.: Updating Markov chain models using the ensemble Kalman Filter. Comput. Geosci. **15**(2), 325–344 (2011). doi:10.1007/s10596-010-9220-4
29. Riva, M., Guadagnini, A., Fernandez-Garcia, D., Sanchez-Vila, X., Ptak, T.: Relative importance of geostatistical and transport models in describing heavily tailed breakthrough curves at the Lauswiesen site. J. Contam. Hydrol. **101**(1–4), 1–13 (2008). doi:10.1016/j.jconhyd.2008.07.004
30. Sebacher, B., Hanea, R., Heemink, A.: A probabilistic parametrization for geological uncertainty estimation using the ensemble Kalman filter (EnKF). Comput. Geosci. **17**(5), 813–832 (2013). doi:10.1007/s10596-013-9357-z
31. Stien, M., Kolbjørnsen, O.: Facies modeling using a Markov mesh model specification. Math. Geosci. **43**(6), 611–624 (2011). doi:10.1007/s11004-011-9350-9
32. Strebelle, S.: Conditional simulation of complex geological structures using multiple-point statistics. Math. Geol. **34**(1), 1–21 (2002). doi:doi:10.1023/A:1014009426274
33. Tan, X., Tahmasebi, P., Caers, J.: Comparing training-image based algorithms using an analysis of distance. Math. Geosci. **46**(2), 149–169 (2014). doi:10.1007/s11004-013-9482-1
34. Viterbi, A.J.: Error bounds for convolutional codes and an asymptotically optimum decoding algorithm. IEEE T. Inform. Theory **13**(2), 260–269 (1967). doi:10.1109/TIT.1967.1054010
35. Zhang, T., Switzer, P., Journel, A.: Filter-based classification of training image patterns for spatial simulation. Math. Geol. **38**(1), 63–80 (2006). doi:10.1007/s11004-005-9004-x
36. Zhang, Y., Oliver, D.S., Chen, Y., Skaug, H.J.: Data assimilation by use of the iterative ensemble smoother for 2D facies models. SPE J. **20**(1), 169–185 (2014). doi:10.2118/170248-PA
37. Winter, C.L., Tartakovsky, D.M., Guadagnini, A.: Moment differential equations for flow in highly heterogeneous porous media. Surv. Geophys. **24**(1), 81–106 (2003). doi:10.1023/A:1022277418570